

RESEARCH ARTICLE

Open Access



Wind tunnel and numerical study of outdoor particle dispersion around a low-rise building model

Runmin Zhao¹, Junjie Liu¹, Nan Jiang² and Sumei Liu^{1*}

Abstract

The dispersion of particulate pollutants around buildings raises concerns due to adverse health impacts. Accurate prediction of particle dispersion is important for evaluating health risks in urban areas. However, rigorous validation data using particulate tracers is lacking for numerical models of urban dispersion. Many prior studies rely on gas dispersion data, questioning conclusions due to differences in transport physics. To address this gap, this study utilized a combined experimental and computational approach to generate comprehensive validation data on particulate dispersion. A wind tunnel experiment using particulate tracers measured airflow, turbulence, and particle concentrations around a single building, providing reliable but sparse data. Validated large eddy simulation expanded the data. This combined approach generated much-needed validation data to evaluate numerical particle dispersion models around buildings. Steady Reynolds-averaged Navier–Stokes (SRANS) simulations paired with Lagrangian particle tracking (LPT), and drift-flux (DF) models were validated. SRANS had lower accuracy compared to LES for airflow and turbulence. However, in this case, SRANS inaccuracies did not prevent accurate concentration prediction when LPT or a Stokes drift-flux model were used. The algebraic drift-flux model strongly overpredicted the concentration for large micron particles, indicating proper drift modeling was essential.

Keywords Outdoor particle dispersion, Large eddy simulation, Lagrangian particle tracking, Drift-flux model

1 Introduction

The dispersion of particulate pollutants around buildings raises significant environmental concerns due to the adverse health impacts of exposure to suspended urban particles (Alemayehu et al., 2020). Accurate prediction of particle dispersion is important for evaluating health risks associated with particulate pollutants in urban areas.

Field experiments provide sparse observations and are limited by high costs and difficulty in standardizing testing conditions across measurements (Antoniou et al., 2019; S. Liu et al., 2018; Stathopoulos et al., 2004; Zou et al., 2021). Wind tunnel simulations can provide reliable data under controlled conditions but still bring substantial costs for the tunnel infrastructure and instrumentation (Blocken et al., 2016a, b).

Large-eddy simulation (LES) models accurately predict turbulent urban winds by explicitly resolving turbulent eddies (Blocken, 2018; Mirzaei, 2021; Zheng & Yang, 2021). These resolved eddies also explicitly carry pollutants in a manner closer to actual transport phenomena. However, the fine resolution requires substantial computational resources. As a less demanding alternative for transient simulation, unsteady Reynolds-averaged Navier–Stokes (URANS) modeling reduces cost through

*Correspondence:

Sumei Liu
smliu@tju.edu.cn

¹ Tianjin Key Laboratory of Indoor Air Environmental Quality Control, School of Environmental Science and Engineering, Tianjin University, Tianjin 300072, China

² School of Mechanical Engineering, Tianjin University, Tianjin 300072, China

ensemble-averaged modeling that filters out stochastic turbulence with turbulence models. However, URANS exhibits low-frequency unsteadiness with single-peak spectra for urban simulation, overlooking key multiscale flow behaviors, and significantly underestimating turbulence, especially within building arrays where fluctuations can disappear entirely (Tominaga, 2015; Tominaga & Stathopoulos, 2017). Hybrid URANS-LES can save approximately 20% in mesh and time versus pure LES with comparable accuracy for urban prediction (J. Liu & Niu, 2019). It is still resource-intensive, since the accuracy still relies heavily on resolved turbulence requiring fine mesh resolution, and the model reverts to URANS when under-resolved. Compared to these transient modeling strategies, steady RANS (SRANS) modeling significantly reduces expenses by avoiding expensive time-resolved calculations with further simplified handling of turbulence. However, the single-point closure and ill-conditioned governing equations derived from the time-averaging assumptions degrade accuracy even more (Brener et al., 2021; Girimaji & Abdol-Hamid, 2005; Hao & Gorlé, 2022; Wu et al., 2019; R. Zhao et al., 2022, 2023). Nevertheless, SRANS remains the main workhorse for industrial computational fluid dynamics (CFD) simulations (Blocken, 2014), benefiting from its computational efficiency and widely accepted guidelines (Blocken & Gualtieri, 2012; Blocken et al., 2012; Franke et al., 2011; Tominaga et al., 2008). As SRANS only provides steady-state eddy viscosity and turbulence kinetic energy (TKE) to represent turbulence, the turbulent dispersion of particles must also be modeled using additional sub-models based on analogous assumptions.

Two main approaches exist for outdoor particle dispersion modeling: Lagrangian particle tracking (LPT) (Bahlali et al., 2019; Haghighifard et al., 2018; Oettl, 2015; Trini Castelli et al., 2018) and Eulerian continuum models (Blocken et al., 2016a, b; Karttunen et al., 2020; Niu et al., 2018). Lagrangian particle tracking (LPT) methods model discrete particles subject to various forces (e.g., gravity and drag from computed flow fields), moving them according to Newton's laws. When paired with LES (termed LES-LPT), as resolved eddies transport the numerical particles, the LES-LPT method provides the most realistic particle tracking with the fewest modeling assumptions. When applied with SRANS simulations (termed SRANS-LPT), an additional sub-model, the discrete random walk (DRW) model, is required to incorporate stochastic effects of turbulence on particles based on the simulated airflow and turbulence statistics (Haghighifard et al., 2018; Oettl, 2015). The DRW model simply uses Gaussian random numbers to generate pseudo fluctuation sequences of the airflow velocity, based on the

SRANS output of TKE. The reductionist assumptions made in the DRW model and underlying inaccuracy in SRANS introduce considerable uncertainty for SRANS-LPT modeling. Regardless of the airflow simulation approach, LPT by its nature enables analysis of trajectories, deposition, and retention times. However, the tracking process remains transient even when using steady-state airflow data, and the computational cost grows with the number of particle tracers. Aside from the Lagrangian view, the Eulerian view is another way to model the particle phase, assuming it as a continuum and establishing a convection–diffusion equation for particle concentrations, as for gases (B. Zhao et al., 2009). Despite significantly reducing computational time, one modeling challenge is accounting for particle inertia and gravity, which cause velocity differences between particle and carrier phases, i.e. particle drift. Using the airflow velocity directly in the convection–diffusion equation provides misleading particle concentration flux, requiring extra drift-flux (DF) models (E. M. A. Frederix et al., 2017). Additionally, for application with SRANS (SRANS-DF), turbulence transport of particles can only be based on molecular diffusion assumption (B. Zhao et al., 2009).

Given the SRANS inaccuracy and additional uncertainty in dispersion modeling, rigorously evaluating the performance of SRANS-LPT and SRANS-DF approaches is critical before engineering application. There have been extensive experimental and numerical studies for particle transport in indoor environments (Cao et al., 2018; S. Liu et al., 2022; S. Liu & Deng, 2023; B. Zhao et al., 2009). However, for urban studies, while experimental studies on gaseous tracer dispersion exist (Architectural Institute of Japan, 2008; COST ES, 1006, 2012; Leiti & Schatzmann, 2005), there is a lack of rigorous validation data using particulate tracers. Many prior studies rely on validating particle models against gas dispersion data (Bahlali et al., 2019; Haghighifard et al., 2018; Oettl, 2015; Trini Castelli et al., 2018), which questions the conclusions due to differences in transport physics. The validity of the numerical models for particle dispersion around buildings remains unknown, especially when large particles are considered (E. Frederix, 2016; E. M. A. Frederix et al., 2017).

To provide reliable validation data to evaluate outdoor particle dispersion simulation with SRANS, this study utilizes a combined experimental and high-fidelity simulation approach to generate a comprehensive dataset for particulate dispersion around a single building. First, a detailed wind tunnel experiment is conducted using particulate tracers for concentration measurements. These results are complemented by a validated LES of the same scenario to broaden the reference dataset. SRANS

simulations paired with both Eulerian and Lagrangian particle tracking models are performed and validated against the obtained reference data.

2 Methods

This section describes the wind tunnel experiment, as well as the employed models for turbulence and dispersion.

2.1 Wind tunnel experiment

The wind tunnel experiment was conducted in an open-circuit wind tunnel at Tianjin University, using a test section with dimensions of 0.35 m width by 0.225 m height. To generate atmospheric boundary layer flow, four triangular spires designed based on Irwin’s approach (Irwin, 1979) were installed upstream, along with seven thin horizontal bars attached to the spires to produce the required turbulence intensity, as inspired by the lattice method for simulating part-depth ABL flows (Lee et al., 2004). Downstream of the spires, a fetch of cube-shaped roughness elements with decreasing heights was arranged (Fig. 1a). Iterative adjustments were made to the horizontal bar spacings on the spires and layout of the roughness cubes until the desired ABL velocity profile was achieved. Measurements were conducted using a single-wire constant temperature anemometer (CTA) TSI IFA-300 (Fig. 1b) mounted on a traverse system with a precision of 10 μm (Fig. 1c). The TSI IFA-300 outputs a real-time, continuous analog voltage signal that correlates to the dynamic air velocity fluctuations across its calibrated velocity range. It has a frequency response greater than 250 kHz. For the given single-wire probe

used, the IFA-300 was calibrated for velocities ranging from 0.01 to 30 m/s. Data was acquired at a 40 kHz sampling frequency, collecting 2,097,152 samples at each measurement location over one-minute durations.

The vertical profile of the mean wind velocity of the formulated part-depth ABL flow followed a 0.25 power law (Eq. 1). The profile of the streamwise turbulence intensity I_x matched the empirical equation (Eq. 2) suggested by the American Society of Civil Engineers (ASCE) (American Society of Civil Engineers, 1999), where $\sigma_U(z)$ is the standard deviation of the measured velocity and $z_0 = 1.8 \times 10^{-4}$ m is the regional roughness height. Although some measured turbulence intensity values deviated from the theoretical curve in the upper region, this was acceptable for the validation study, since using the measured profiles rather than theoretical atmospheric boundary layer (ABL) profiles as boundary conditions is common practice. The measured velocity and turbulence intensity profiles of the wind tunnel flow used as boundary conditions are shown in Fig. 2.

$$\frac{U(z)}{U_H} = \left(\frac{z}{H}\right)^{0.25} \tag{1}$$

$$I_x(z) = \frac{\sigma_U(z)}{U(z)} = \frac{1}{\ln(z/z_0)} \tag{2}$$

After generating the desired atmospheric boundary layer (ABL) flow, a 2:2:1 building model was positioned where the incident ABL flow measurements were taken, with its windward face perpendicular to the wind direction.

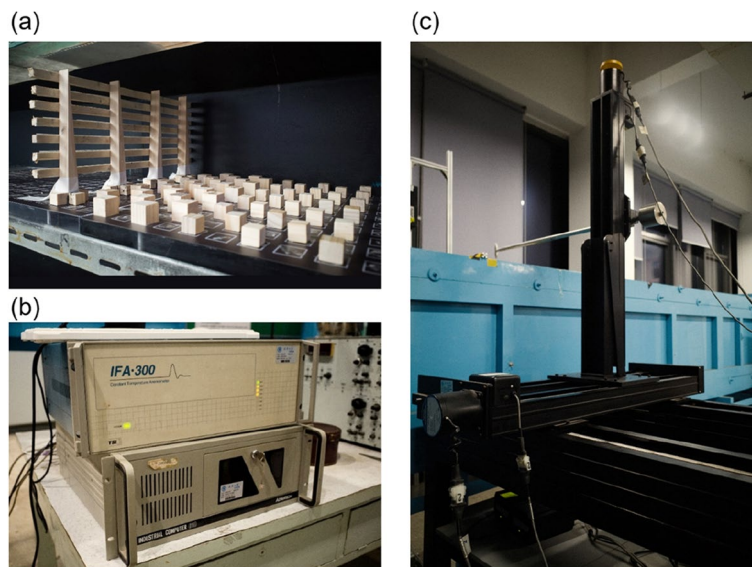


Fig. 1 a Spires and roughness elements; b Constant temperature anemometer; c Traverse system

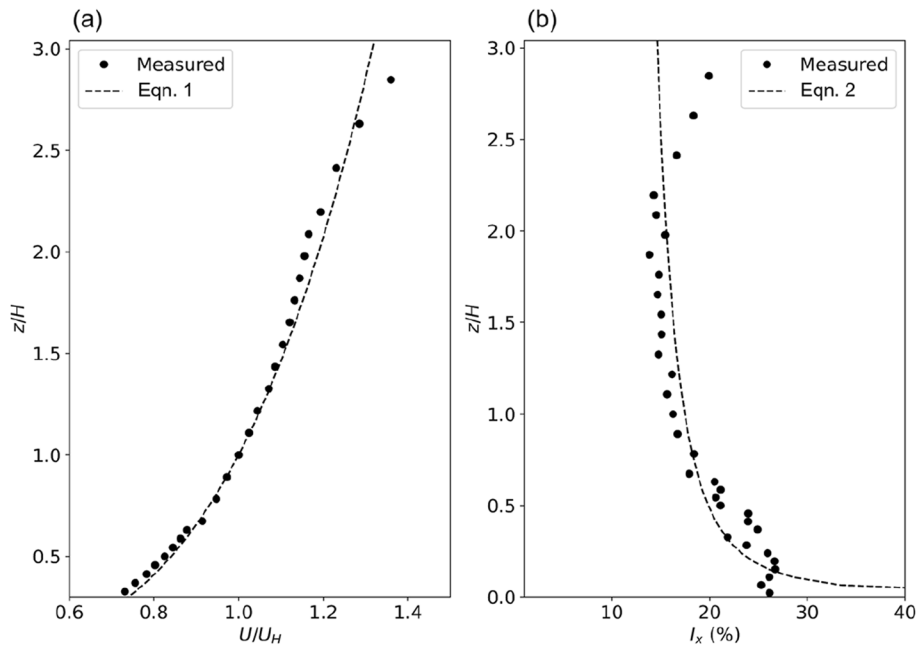


Fig. 2 Profiles of **a** velocity and **b** turbulence intensity of the formulated part-depth ABL flow in the wind tunnel

The building model dimensions were 0.09 m length, 0.09 m width, and 0.045 m height (H), so the reference wind speed of $U_H = 14.5$ m/s ensured a building Reynolds number of $Re = U_H H / \nu = 43,500$. Hot-wire anemometer measurements were taken along nine vertical sample lines surrounding the building model, as illustrated in the schematic in Fig. 3. The measurements around the building were repeated three times on different dates and averaged to obtain the final values used.

After establishing reproducible atmospheric boundary layer (ABL) flow and building airflow patterns, an additional experiment was performed to measure particle dispersion from a roof stack. A diethylhexyl sebacate

(DEHS) particle generator was used to produce a particle flow for the dispersion experiments (see Fig. 4a). The generator flow rate was controlled by an air pump and monitored with a flow meter. The DEHS generator output was connected via silicone tubing to a seamless steel tube (8 mm outer diameter, 6 mm inner diameter). This steel tube was inserted through an 8 mm diameter hole made in the center of the building model and protruded 6 mm above the roof level as a roof stack, as visualized in Fig. 4b. This particle injection setup enabled the DEHS particles from the generator to be emitted through the roof stack with manually controlled flow rate and thus a constant injection velocity W_e from the roof stack.

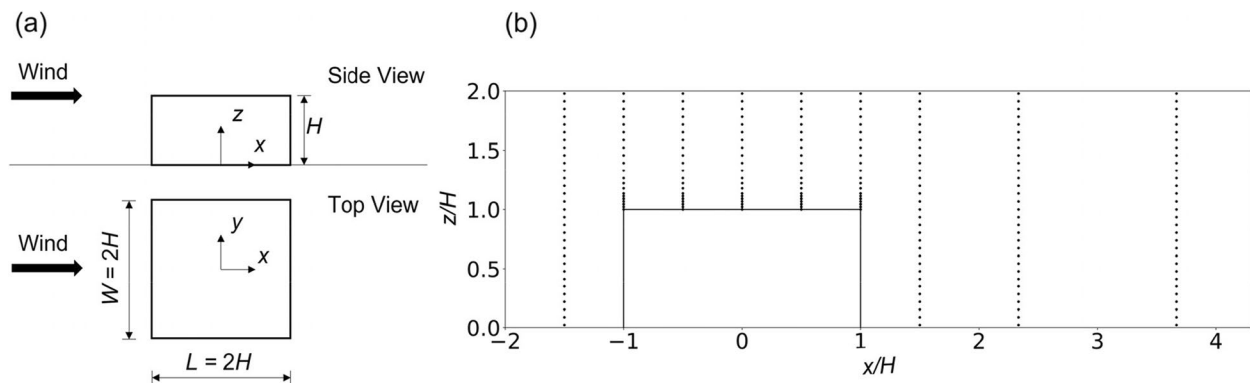


Fig. 3 **a** Schematic of the wind tunnel experiment; **b** measurement locations for velocity and turbulence

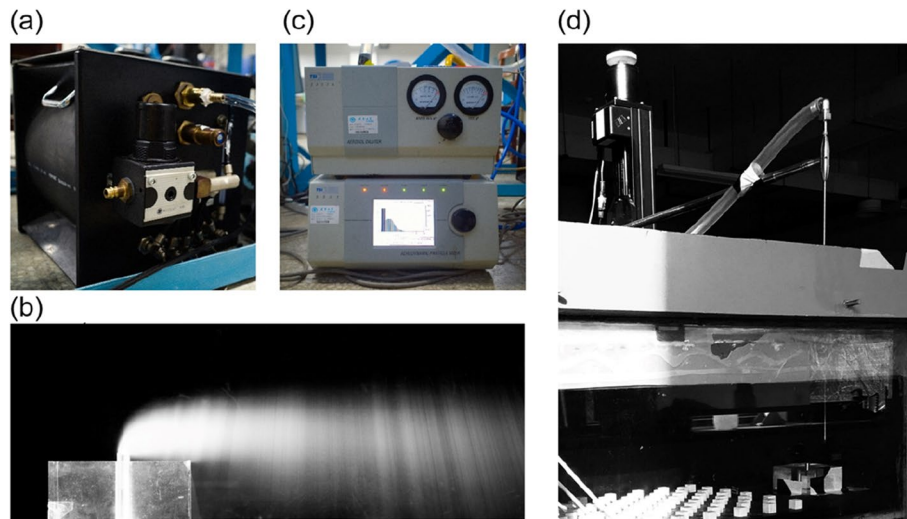


Fig. 4 **a** DEHS generator; **b** visualization of the particle injection; **c** Aerodynamic Particle Sizer APS 3321 and Aerosol Diluter 3302A; **d** Particle collection tube mounted on the traverse system

Particle concentration measurements were conducted using an Aerodynamic Particle Sizer (TSI APS 3321) and an Aerosol Diluter (TSI 3302A) set to a 100:1 dilution ratio. The APS 3321 simultaneously counts particles from 0.5 to 20 μm aerodynamic diameter in 32 size channels. Concentrations up to 1000 particles/ cm^3 can be measured at 0.5 μm with a coincidence of less than 2% and at 10 μm with a coincidence under 6%. Usable data are provided up to 10,000 particles/ cm^3 . The size resolution is 0.02 μm at 1.0 μm and 0.03 μm at 10 μm . The minimum detectable concentration is 0.001 particle/ cm^3 . The accuracy is $\pm 10\%$ plus counting variations. The maximum processing rate exceeds 200,000 particles/s. The accompanying 3302A diluter offers 100:1 and 20:1 sample dilution at a 5 L/min flow rate drawn by the spectrometer. For respirable particles, it has a penetration efficiency over 93%, with lower efficiency for larger sizes. Efficiency corrections are built into the software. Particles were

sampled iso-kinetically using a 3 mm diameter seamless steel tube with an angled tip at the lower end. The upper end of the sampling tube was connected to 19 mm silicone tubing and mounted on a traverse system, allowing controlled movement of the sampling assembly (Fig. 4d). This measurement setup enabled diluted particle sampling with precise position control to obtain concentration measurements around the building model. A schematic of the dispersion experiment and particle sampling locations is given in Fig. 5. Two W_e values ($W_e = U_H$ and $W_e = 2U_H$) were considered in the measurements.

2.2 Governing equations and turbulence modeling

The previous subsection outlined the wind tunnel experiment, this subsection describes the SRANS and LES approaches for the reproduction of airflow and turbulence around the building model.

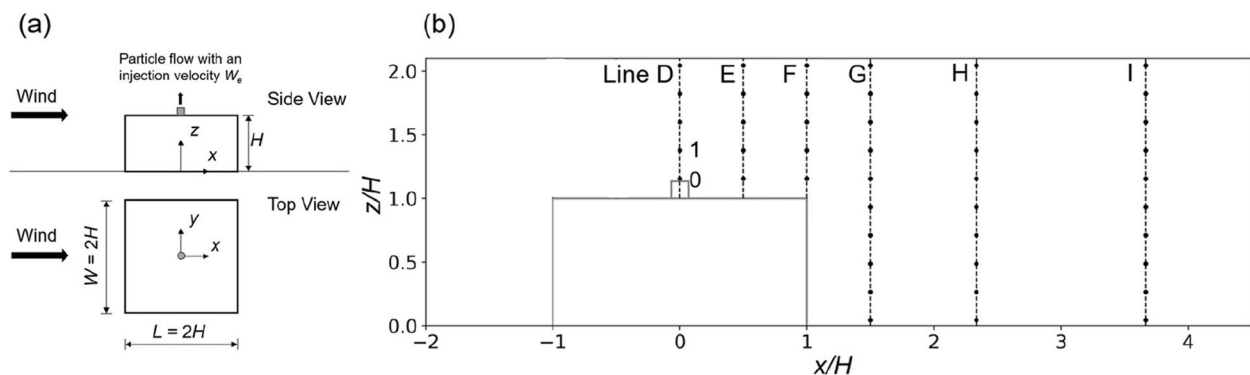


Fig. 5 **a** Schematic of the dispersion experiment; **b** sampling locations for particle concentration, with Lines D-I and points 0 and 1 defined

Alongside the continuity equation for velocity (Eq. 3), the governing equations for velocity and turbulence can be written in a general form (Eq. 4), where U_i, U_j are the mean (SRANS) or filtered (LES) velocity components, in the x_i, x_j directions ($i, j = 1, 2, 3$). ϕ is the transported quantity, Γ is the diffusion coefficient of ϕ , and S_ϕ is the source term. Table 1 summarizes the model equations for SRANS with Kato-Launder (KL) $k-\varepsilon$ model (Kato & Launder, 1993) and LES with wall-adapting local eddy-viscosity (WALE) model (Nicoud & Ducros, 1999). Previous studies have provided comprehensive evaluations comparing the performance of different SRANS turbulence models for urban airflow and gaseous concentration prediction (Gousseau et al., 2011; Toja-Silva et al., 2015; Tominaga & Stathopoulos, 2007, 2010; Vardoulakis et al., 2011; Yoshie et al., 2007; R. Zhao et al., 2022, 2023). Though the various SRANS models differ, their discrepancies were small relative to differences with LES or experimental data, since all SRANS models showed poor accuracy, especially for TKE. This study selects the KL model as representative of SRANS performance. It introduces a production limiter to the standard $k-\varepsilon$ model to mitigate the unphysical generation of in impingement regions. For LES, provided a sufficiently fine resolution mesh is used, the choice of sub-grid scale model contributes only negligible differences, according to Okaze et al. (Okaze et al., 2021). Thus, this study employs the numerically stable WALE model.

$$\frac{\partial U_j}{\partial x_j} = 0 \tag{3}$$

$$\frac{\partial \phi}{\partial t} + U_j \frac{\partial \phi}{\partial x_j} = \Gamma \frac{\partial^2 \phi}{\partial x_j \partial x_j} + S_\phi \tag{4}$$

In Table 1, ν and ν_t are the kinematic viscosity and turbulence viscosity. p is the pressure, and ρ is the density.

k is TKE, P_k is the turbulence production term, ε is the turbulence dissipation rate, S_{ij} is the strain rate tensor, Ω_{ij} is the rotation rate tensor, δ_{ij} is the Kronecker Delta function.

2.3 Dispersion modeling

Based on the airflow and turbulence solved using the approaches described above, this subsection describes the LPT and DF approaches for the simulation of particle dispersion.

For LPT, the position of a particle $x_{p,i}$ and its velocity $u_{p,i}$ are tracked by the following equation system (Eqs. 5-6), where ρ_p is the particle density, d_p is the particle diameter, C_D is the drag coefficient, Re_p is the particle Reynolds number. U_i and U'_i are the mean and fluctuating velocity of air. Here only the drag force and gravitational force are considered.

$$\frac{dx_{p,i}}{dt} = u_{p,i} \tag{5}$$

$$\frac{du_{p,i}}{dt} = \frac{18\rho\nu}{\rho_p d_p^2} \frac{C_D Re_p}{24} [(U_i + U'_i) - u_{p,i}] + \left(1 - \frac{\rho}{\rho_p}\right) g_i \tag{6}$$

Re_p is calculated using Eq. 7 and C_D is obtained using Eq. 8 (Putnam, 1961).

$$Re_p = \frac{|(U_i + U'_i) - u_{p,i}| d_p}{\nu} \tag{7}$$

$$C_D = \begin{cases} \frac{24}{Re_p} \left(1 + \frac{1}{6} Re_p^{\frac{2}{3}}\right), & Re_p < 1000 \\ 0.44, & Re_p > 1000 \end{cases} \tag{8}$$

LES directly simulates the fluctuating velocity U'_i in both space and time, while SRANS can only obtain U_i with turbulence represented by k and ε . The discrete random walk (DRW) model (Eqs. 9-10) is a viable approach

Table 1 Coefficients and source terms

	ϕ	Γ	S_ϕ	Constants and coefficients
SRANS with KL model (Kato & Launder, 1993)	U_i	$\nu + \nu_t$	$-\frac{1}{\rho} \frac{\partial p}{\partial x_i}$	$\nu_t = C_\mu \frac{k^2}{\varepsilon}$; $P_k = \nu_t S_{ij} \Omega_{ij}$; $S = \sqrt{2 S_{ij} S_{ij}}$; $\Omega = \sqrt{2 \Omega_{ij} \Omega_{ij}}$; $C_\mu = 0.09, C_{\varepsilon 1} = 1.44, C_{\varepsilon 2} = 1.92,$ $\sigma_k = 1.0,$ and $\sigma_\varepsilon = 1.3$
	k	$\nu + \frac{\nu_t}{\sigma_k}$	$P_k - \varepsilon$	
	ε	$\nu + \frac{\nu_t}{\sigma_\varepsilon}$	$\frac{C_{\varepsilon 1} P_k \varepsilon}{k} - \frac{C_{\varepsilon 2} \varepsilon^2}{k}$	
LES with WALE model (Nicoud & Ducros, 1999)	U_i	$\nu + \nu_t$	$-\frac{1}{\rho} \frac{\partial p}{\partial x_i}$	$\nu_t = (C_w \Delta)^2 \frac{(S_{ij}^d S_{ij}^d)^{\frac{3}{2}}}{(S_{ij} S_{ij})^{\frac{5}{2}} + (S_{ij}^d S_{ij}^d)^{\frac{3}{2}}}$; $S_{ij}^d = \frac{1}{4} \left(\frac{\partial U_i}{\partial x_j} + \frac{\partial U_j}{\partial x_i} \right)$; $S_{ij}^d = \frac{1}{2} \left(\frac{\partial U_k}{\partial x_j} \frac{\partial U_j}{\partial x_k} + \frac{\partial U_k}{\partial x_i} \frac{\partial U_i}{\partial x_k} \right) - \frac{1}{3} \delta_{ij} \frac{\partial U_k}{\partial x_k}$; $C_w = 0.325$

to construct spatial and temporal sequence of U'_i from the turbulence statistics using normal random numbers λ_i (OpenCFD Ltd., 2020).

$$U'_i = \lambda_i \sqrt{\frac{2k}{3}} \quad (9)$$

$$t_{inter} = \min\left(\frac{k}{\varepsilon}, 0.164 \frac{k^{1.5}}{\varepsilon |U_i + U'_i| - u_{p,i}}\right) \quad (10)$$

The particle interacts with the fluid over a particle interaction timescale t_{inter} with a constant U'_i value. After each interaction time has elapsed, a new U'_i value is obtained by generating new λ_i values.

In an Eulerian perspective, the particle concentration follows a species transport equation (Eq. 11). For particles, the diffusion is only related to turbulence and $Sc_t=1$ (B. Zhao et al., 2009).

$$\frac{\partial [(U_j + u_{drift,j})C]}{\partial x_j} = \frac{\partial}{\partial x_j} \left(\frac{v_t}{Sc_t} \frac{\partial C}{\partial x_j} \right) \quad (11)$$

To obtain the inertial drift velocity $u_{drift,i} = u_{p,i} - U_i$, the local equilibrium assumption, as described by Manninen et al. (Manninen et al., 1996), can be adopted. Under this assumption, the inertial drift velocity can be modeled using an algebraic drift-flux model (ADF) as (E. M. A. Frederix et al., 2017):

$$u_{drift,j} = \tau \left(1 - \frac{\rho}{\rho_p} \right) g_i \quad (12)$$

$$\tau = \frac{\rho_p d_p^2}{18 \rho \nu} \quad (13)$$

However, the assumption does not necessarily hold for particles with large Stokes numbers (E. Frederix, 2016), for which the Stokes drift-flux model (SDF) should be

applied for accurate modeling of the drift velocity (E. M. A. Frederix et al., 2017).

$$(u_{drift,j} + U_j) \frac{\partial (u_{drift,j} + U_j)}{\partial x_j} = -\frac{1}{\tau} u_{drift,i} + \left(1 - \frac{\rho}{\rho_p} \right) g_i \quad (14)$$

2.4 Case setup

This subsection describes the computational domain, mesh generation, and numerical setups of the CFD simulations.

The computational domain was set following the AIJ guidelines (Tominaga et al., 2008). The distances from the building to the inlet, the sides, and the top of the domain were all set as $5H$, and the distance to the outlet was $10H$. Computational grids of the three cases were generated by the open-source mesh generation tool snappyHexMesh. The cells adjacent to the building surface had a size of $H/40$. A refinement box extending streamwise from $-2H$ to $4H$, spanwise from $-2H$ to $2H$, and vertically from 0 to $2H$ was designated to match the dimensions of the measurement region. Within this refinement box, 20 levels of boundary layers were generated from the building surface, with the first layer having a thickness of $H/1500$ and a growth rate of 1.15. The mesh maintained a size of $H/40$ and was then coarsened to $H/10$ in a larger refinement box extending streamwise from the inlet plane to $6H$, spanwise from $-3H$ to $3H$, and vertically from 0 to $3H$. The background mesh outside of the refinement boxes had a cell size of $H/2$. The mesh sizes and boundary layer settings are essentially identical to the finest LES setup in Z. Liu et al. (Z. Liu et al., 2020) for a same 2:2:1 model. The mesh details are shown in Fig. 6.

The simulations were conducted in the open-source code OpenFOAM-v2012 (OpenCFD Ltd., 2020). The inlet boundary conditions for velocity (U) and turbulence kinetic energy (k) were directly imposed by interpolating the measured profiles of the incident wind tunnel flow. The inlet turbulence dissipation rate (ε) profile was calculated from U and k using empirical

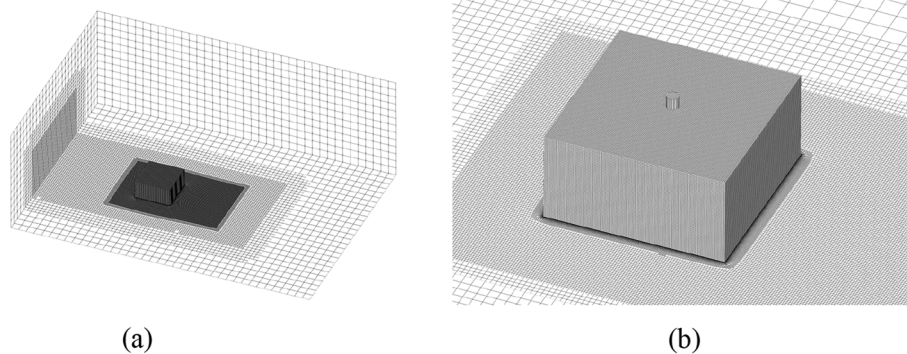


Fig. 6 **a** Overview and **b** regional view of mesh

equations suggested by Mochida et al. (Mochida et al., 2002). For LES simulation, the prescribed profiles were used as inputs for the inlet turbulence generator, a divergence-free synthetic eddy method (DFSEM) boundary condition, as provided in OpenFOAM. Symmetry boundary conditions were applied at the side and top boundaries. For building surfaces, standard wall functions were used. For ground surfaces, z_0 -type wall functions as suggested in Richards and Hoxey (Richards & Hoxey, 1993) were used in SRANS simulations while standard wall functions were for LES. The roughness length (z_0) values were estimated from the measured U and k values closest to the ground in the incident flow (Mochida et al., 2002). Other boundary conditions are listed in Tables 2 and 3 for clarity.

To solve for LES in combination with LPT, the kinematicParcelFoam solver based on the PIMPLE algorithm was employed. Since LES directly resolves the fluctuating velocity, no DRW model was used. The central linear scheme was applied for gradient terms and Laplacian terms. For the divergence terms, A filtered linear scheme was used for U . To replicate the measurement process using a single-wire probe placed perpendicular to the $y=0$ plane, the effective velocity U_{eff} is approximated as shown in Eq. 15, following the approach of Fischer et al. (Fischer et al., 2022). Since U_y is aligned parallel to the wire, it has a minimal effect on the cooling of the hotwire. In contrast, U_z is aligned perpendicular to the wire and therefore influences the cooling similarly as the primary flow component U_x . The simulations were run for six flow-through times in the computational domain with a temporal resolution of 40 kHz, matching the hot-wire measurements. This small time step of 2.5×10^{-5} s ensures an average Courant–Friedrichs–Lewy (CFL) number well below 0.1. The first pass allowed for a spin-up of the flow field. The airflow and concentration data from the subsequent five passes were averaged to obtain the mean and variance statistics.

$$U_{eff} = \sqrt{(U_x^2 + 0.01U_y^2 + U_z^2)}. \tag{15}$$

Table 2 Boundary conditions for LES and SRANS

	LES	SRANS
Injection	Prescribed velocity W_e	Prescribed velocity W_e
Inlet	Inflow turbulence generated by DFSEM, based on prescribed velocity and Reynolds stress profile	Prescribed U, k , and ϵ
Solid walls	No slip with standard wall function	No slip with standard wall function
Ground	No slip with standard wall function	No slip with z_0 -type roughness wall function
Sides/Top	Symmetry	Symmetry
Outlet	Fixed for pressure and zero-gradient other quantities	Fixed for pressure and zero-gradient other quantities

Table 3 Boundary conditions for DF and LPT

	DF	LPT
Injection	Fixed value	Fixed particle injection rate (10^7 particles/s)
Inlet	Zero-gradient	Reflect
Solid walls	Zero-gradient	Escape
Ground	Zero-gradient	Escape
Sides/Top	Symmetry	Escape
Outlet	Zero-gradient	Escape

The simpleFoam solver based on the SIMPLE algorithm was employed to solve for SRANS. For the divergence terms, the second-order upwind scheme was used for U , the Van Leer scheme for k and ϵ . The simulations were of second-order accuracy. The convergence criterion was 10^{-4} for the residuals of all the variables. Based on the steady-state results for the airflow and turbulence field, the DF models were solved using an implemented drift-flux solver. LPT was performed using kinematicParcelFoam with a transient time-averaging process as was done in LES, but with a fixed airflow field, and a DRW model (Eq. 9) to estimate the fluctuating velocity.

3 Results

This section presents the airflow, turbulence, and particle concentration measurements from the wind tunnel experiment, along with validation of LES and SRANS against this experimental data.

3.1 Validation of airflow and turbulence

Figure 7 compares the effective velocity $\overline{U_{eff}}$ and variance of effective velocity $\sigma(U_{eff})$ measured using the single-wire CTA and simulated using LES with the numerical probe (Eq. 15). LES accurately simulated the mean statistics of airflow and turbulence, except for minor differences above the roof height.

Since the effective velocity cannot be resolved in SRANS, the validated LES data was used as a reference

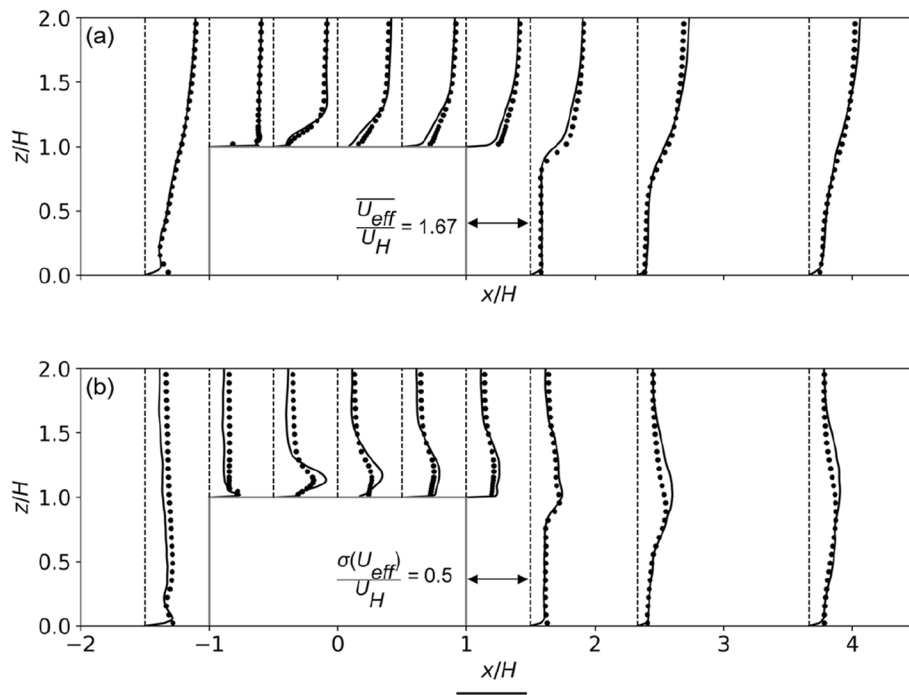


Fig. 7 Comparison of **a** mean effective velocity $\overline{U_{eff}}$ and **(b)** variance of effective velocity $\sigma(U_{eff})$ measured (points) and predicted by LES (solid line)

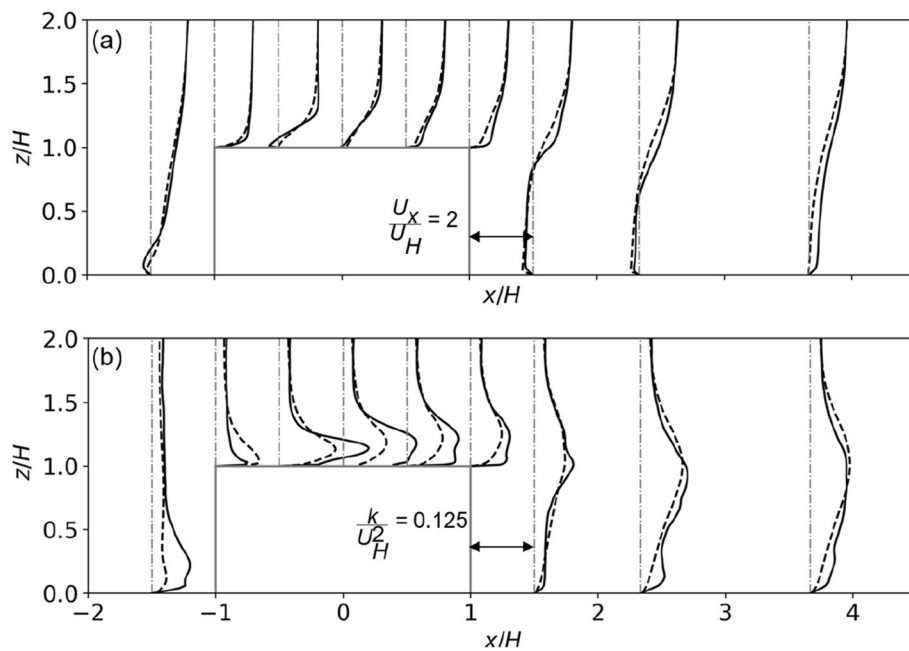


Fig. 8 Comparison of time-averaged **a** stream-wise velocity component, and **b** TKE predicted by SRANS (dashed) and LES (solid)

to reconstruct the full velocity components. Figures 8–10 compare the velocity components and TKE obtained from SRANS and LES. In Fig. 8a, the SRANS streamwise velocity differs from LES results mainly in the rooftop and far-wake regions, indicating an inaccurate prediction

of the separation. This is more clearly observed in Fig. 9, with SRANS showing a significantly overpredicted wake reattachment length. Figure 8b shows SRANS underpredicting TKE on the roof and in the far-wake region, also evident in Fig. 10.

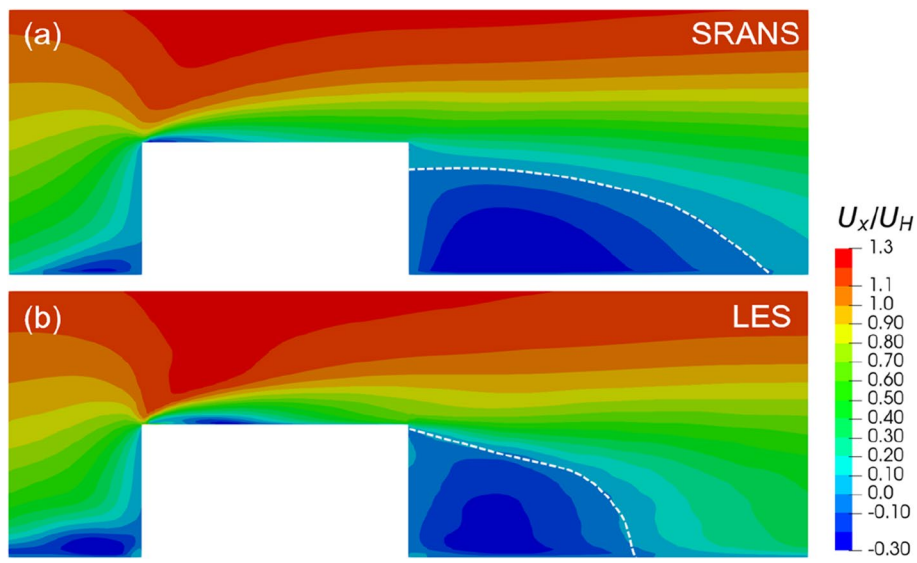


Fig. 9 Comparison of contours of time-averaged stream-wise velocity predicted by **a** SRANS and **b** LES

3.2 Validation of dispersion models

Figure 11 compares the simulated particle concentrations for $d_p=1 \mu\text{m}$ to the measured values under the condition $W_e/U_H=1$. The concentrations were normalized by the value at the nozzle opening (C_0 at point 0). Overall, LES was the most accurate in this case, while the other SRANS-based models also showed reasonable agreement with the experimental data. Results from SRANS-ADF and SRANS-SDF were identical and deviated most from measurements, especially downstream of the building (Lines G-I). The overpredicted concentrations

indicate insufficient particle dispersion, explainable by the underpredicted TKE and thus v_t (see Eq. 11). However, SRANS-LPT aligned well at Lines G and H, despite slightly underpredicting at Line I, suggesting the DRW suitably compensated for the low TKE here. All models lacked accuracy at Lines E and F.

Figure 12 compares the simulated particle concentrations for $d_p=1 \mu\text{m}$ and $10 \mu\text{m}$ to the measured values under the condition $W_e/U_H=2$. Due to uncertainties in the inlet concentration measurement at the nozzle caused by the high particle count, the concentration

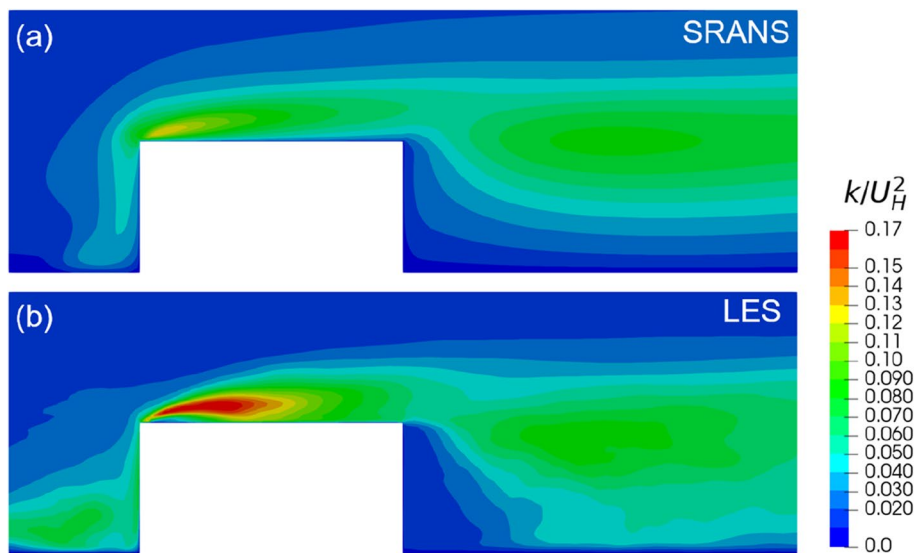


Fig. 10 Comparison of contours of TKE predicted by **a** SRANS and **b** LES

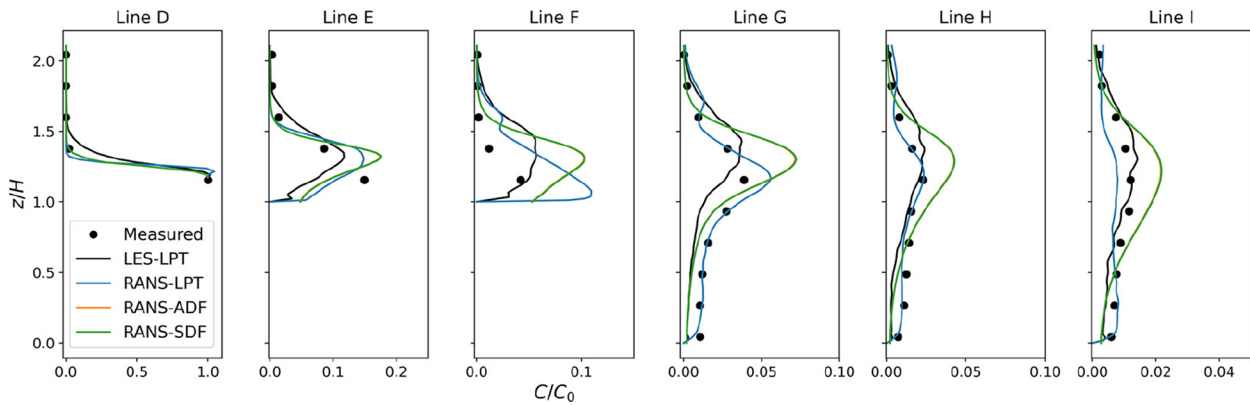


Fig. 11 Comparison of normalized particle concentration using LES-LPT and SRANS paired with LPT, algebraic drift-flux (ADF), and Stokes drift-flux (SDF). $W_e/U_H=1, d_p=1 \mu\text{m}$

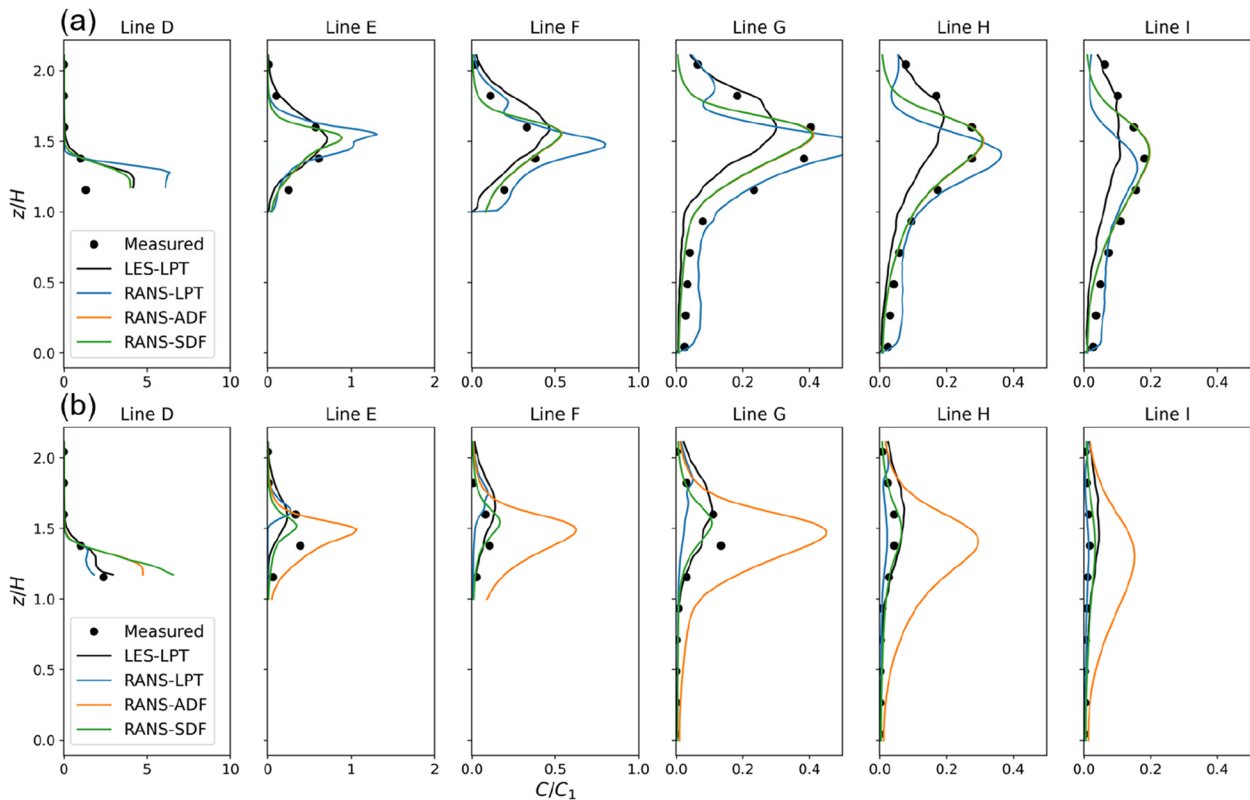


Fig. 12 Comparison of normalized particle concentration using LES-LPT, SRANS-LPT, as well as RANS with algebraic drift-flux (ADF) or Stokes drift-flux (SDF). **a** $W_e/U_H=2, d_p=1 \mu\text{m}$ and **b** $W_e/U_H=2, d_p=10 \mu\text{m}$

above the nozzle opening (C_1 at point 1) was used as the reference for normalization. Again, all the approaches, except for SRANS-ADF, showed a reasonable prediction of the concentration for both particle diameters. In Fig. 12a, SRANS-ADF and SRANS-SDF results remained identical and aligned best with experiments in terms of peak concentrations and positions. Overall,

LES-LPT tended to underpredict concentrations with a higher peak position, while SRANS-LPT overpredicted with a lower peak position. The estimated nozzle concentration by LES-LPT in this case was $C_0 = 4.5C_1$, significantly larger than the measured C_0 . SRANS-ADF and SRANS-SDF also predicted the same nozzle concentration value while SRANS-LPT overpredicted it.

In Fig. 12b, SRANS-ADF strongly overpredicted the concentration, with similar values obtained for the large particles as for the small particles in Fig. 12a. SRANS-SDF continued to closely match the experimental value. LES-LPT also predicted well, while SRANS-LPT was the most inaccurate, generally underpredicting the concentration. The estimated nozzle concentration by LES-LPT and SRANS-LPT in this case was close to the measured C_0 . SRANS-ADF and SRANS-SDF overpredicted the value.

Figure 13 provides a visual comparison of the particle distributions obtained from LPT using SRANS versus LES. The SRANS-LPT leads to a smooth particle distribution that follows an overall Gaussian profile, lacking detailed resolution. Many particles rise to unrealistic elevations in unimpeded random walks. In contrast, the LES-LPT particle distribution appears more realistic. Particles are shown to be carried by coherent turbulent eddies. The dispersion follows a more constrained distribution at lower elevations. This showcases the ability of LES to simulate particle interaction with large flow structures more realistically. Although SRANS-LPT can reasonably simulate the overall particle concentration in a statistical sense (Figs. 11, 12), the individual particle trajectories and reachability are questionable due to the simplified random-walk modeling.

4 Discussion

The raw measurements could not directly evaluate SRANS models due to instrumentation constraints. However, the high-fidelity LES reconstructed flow fields and particle concentrations beyond the experiments' limitations in a complementary manner. Due to single-wire

CTA instrumentation limitations, only positive velocity values could be measured, so the full three-dimensional velocity vector was unobtainable. Also, instrumentation limitations in the particle experiments prevented high-quality measurements of particle concentrations and size distributions in some scenarios. The $W_e/U_H=1$ condition lacked data for 10 μm particles since the injection velocity was low for enough generation of DEHS particles and large particle concentrations were negligible. For $W_e/U_H=2$, the DEHS generator's doubled flow rate caused particle concentrations to exceed the APS's upper detection limit at the nozzle opening (point 0), even with 100:1 dilution. Therefore, the second nearest point from the nozzle opening (point 1) was chosen instead for normalization. Ideally, the $W_e/U_H=1$ case should apply consistent normalization using the same point. However, this is not possible since the measured concentration at point 1 for $W_e/U_H=1$ is a near-zero value not suitable as a denominator. Despite the inconsistency in this normalization between cases, the normalization within each case is consistent for the evaluated models, allowing a fair evaluation. This further stresses the importance of the LES data providing a highly feasible baseline to determine an appropriate normalization approach, enhancing the usability of the experimental data.

SRANS-ADF was not able to correctly model the particle drift for large particles. The calculated drift velocity is very small using Eq. 12. The result is almost identical to a passive scalar modeling of gas dispersion. So the conclusions in previous studies hold only for fine particles since tracer gas data were employed for validation (Bahlali et al., 2019; Haghhighifard et al., 2018; Oettl, 2015; Trini Castelli et al., 2018).

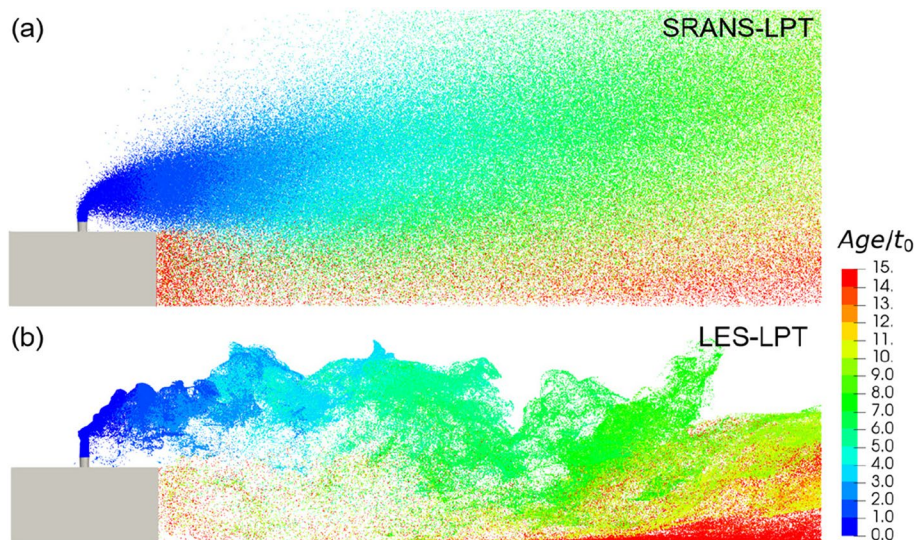


Fig. 13 Particle distribution at $t = 200t_0$ by **a** SRANS-LPT **b** LES-LPT. Colored by particle age normalized by $t_0 = H/U_H$

LES-LPT demonstrated consistent performance across the simulated cases, whereas SRANS-LPT and SRANS-SDF showed varying tendencies between scenarios. This discrepancy stemmed from differences in the tracking mechanisms. LES-LPT did not employ a DRW model. Particles were dispersed solely by explicitly resolved eddies. Uncertainties mainly arose from resolved airflow and turbulence interactions between the jet, inflow, and building-induced flow. For SRANS-LPT, uncertainties originated not only from inaccurate mean airflow and underpredicted TKE but also from the reductionist DRW model approximating eddy strength and duration. For the simplified models, errors from multiple sources could cancel out or strengthen each other in a case-dependent manner. These compensations were not generalizable. Nevertheless, the simplified models were computationally efficient and can be employed for rapid prediction of particle concentrations.

In this experiment, particles were injected from a high-speed roof-stack jet. Whether the conclusions hold for other scenarios, such as ground-level releases in the building wake, remains an open question. Future studies will conduct additional experimental investigations across more scenarios.

5 Conclusions

This study conducted wind tunnel measurements of airflow, turbulence, and particle dispersion around a single low-rise building. Large eddy simulation (LES) validated by the measurements was used to expand the data. Eulerian and Lagrangian methods paired with steady Reynolds-averaged Navier–Stokes (SRANS) were evaluated for predicting outdoor particle dispersion. This study led to the following findings:

LES had superior accuracy for modeling airflow, turbulence, and particle dispersion around a single building. The high time-resolution transient simulation enabled replicating the measurement process of the single-wire CTA and helped infer the high concentrations around the injection nozzle that could not be directly measured in the experiment.

SRANS had lower accuracy for predicting airflow and turbulence around the low-rise building, featuring an extended wake recirculation zone and underpredicted TKE. However, in this case, these inaccuracies did not prevent SRANS from generating accurate particle concentration predictions when Lagrangian particle tracking (LPT) was used. The predicted concentration was close to the LES prediction. However, the individual particle trajectories and reachability are questionable due to the simplified random-walk modeling.

For the Eulerian drift-flux simulations based on the SRANS results, the Stokes drift-flux model accurately

predicted the dispersion of both small 1-micron and large 10-micron particles downstream of the stack. The algebraic drift-flux model accurately predicted the dispersion of the small particles but failed for the large particles. Proper drift modeling was essential for Eulerian prediction in this case, especially for the particles with large Stokes numbers.

Acknowledgements

This study was supported by the National Natural Science Foundation of China (NSFC) through grant No. 52108084.

Authors' contributions

Runmin Zhao: Visualization, Validation, Software, Methodology, Investigation, Formal analysis, Data curation, Writing – original draft. Sumei Liu: Funding acquisition, Resources, Supervision, Writing – review & editing. Junjie Liu: Supervision, Resources, Project administration, Methodology. Nan Jiang: Conceptualization, Methodology, Resources, Supervision.

Declarations

Competing interests

The authors declare that they have no competing interests.

Received: 21 November 2023 Accepted: 21 December 2023

Published online: 08 January 2024

References

- Almeyeh, Y. A., Asfaw, S. L., & Terfie, T. A. (2020). Exposure to urban particulate matter and its association with human health risks. *Environmental Science and Pollution Research*, 27(22), 27491–27506. <https://doi.org/10.1007/s11356-020-09132-1>
- American Society of Civil Engineers. (1999). *Wind tunnel studies of buildings and structures*. American Society of civil engineers.
- Antoniou, N., Montazeri, H., Neophytou, M., & Blocken, B. (2019). CFD simulation of urban microclimate: Validation using high-resolution field measurements. *Science of the Total Environment*, 695. <https://doi.org/10.1016/j.scitotenv.2019.133743>
- Architectural Institute of Japan. (2008). *Guidebook for CFD predictions of urban wind environment*. https://www.ajj.or.jp/jpn/publish/cfdguide/index_e.htm
- Bahlali, M. L., Dupont, E., & Carissimo, B. (2019). Atmospheric dispersion using a Lagrangian stochastic approach: Application to an idealized urban area under neutral and stable meteorological conditions. *Journal of Wind Engineering and Industrial Aerodynamics*, 193(August 2018), 103976. <https://doi.org/10.1016/j.jweia.2019.103976>
- Blocken, B. (2014). 50 years of Computational Wind Engineering: Past, present and future. *Journal of Wind Engineering and Industrial Aerodynamics*, 129, 69–102. <https://doi.org/10.1016/j.jweia.2014.03.008>
- Blocken, B. (2018). LES over RANS in building simulation for outdoor and indoor applications: A foregone conclusion? *Building Simulation*, 11(5), 821–870. <https://doi.org/10.1007/s12273-018-0459-3>
- Blocken, B., & Gualtieri, C. (2012). Ten iterative steps for model development and evaluation applied to Computational Fluid Dynamics for Environmental Fluid Mechanics. *Environmental Modelling and Software*, 33, 1–22. <https://doi.org/10.1016/j.envsoft.2012.02.001>
- Blocken, B., Janssen, W. D., & van Hooff, T. (2012). CFD simulation for pedestrian wind comfort and wind safety in urban areas: General decision framework and case study for the Eindhoven University campus. *Environmental Modelling and Software*, 30, 15–34. <https://doi.org/10.1016/j.envsoft.2011.11.009>
- Blocken, B., Stathopoulos, T., & van Beeck, J. P. A. J. (2016a). Pedestrian-level wind conditions around buildings: Review of wind-tunnel and CFD techniques and their accuracy for wind comfort assessment. *Building and Environment*, 100, 50–81. <https://doi.org/10.1016/j.buildenv.2016.02.004>

- Blocken, B., Vervoort, R., & van Hooff, T. (2016b). Reduction of outdoor particulate matter concentrations by local removal in semi-enclosed parking garages: A preliminary case study for Eindhoven city center. *Journal of Wind Engineering and Industrial Aerodynamics*, 159(October), 80–98. <https://doi.org/10.1016/j.jweia.2016.10.008>
- Brener, B. P., Cruz, M. A., Thompson, R. L., & Anjos, R. P. (2021). Conditioning and accurate solutions of Reynolds average Navier-Stokes equations with data-driven turbulence closures. *Journal of Fluid Mechanics*, 915, 1–27. <https://doi.org/10.1017/jfm.2021.148>
- Cao, Q., Chen, C., Liu, S., Lin, C. H., Wei, D., & Chen, Q. (2018). Prediction of particle deposition around the cabin air supply nozzles of commercial airplanes using measured in-cabin particle emission rates. *Indoor Air*, 28(6), 852–865. <https://doi.org/10.1111/ina.12489>
- COST ES1006. (2012). *Evaluation, Improvement and Guidance for the Use of Local-scale Emergency Prediction and Response Tools for Airborne Hazards in Build Environments*.
- Fischer, L., Straußwald, M., & Pftzner, M. (2022). Analysis of Large Eddy Simulations and 1D Hot-Wire Data to Determine Actively Generated Main Flow Turbulence in a Film Cooling Test Rig. *Journal of Turbomachinery*, 144(11), 1–12. <https://doi.org/10.1115/1.4054778>
- Franke, J. J., Hellsten, A., Schlünzen, K. H., Carissimo, B., Schlunzen, K. H., Carissimo, B., Schlünzen, K. H., & Carissimo, B. (2011). The COST 732 Best Practice Guideline for CFD simulation of flows in the urban environment: A summary. *International Journal of Environment and Pollution*, 44(1–4), 419–427. <https://doi.org/10.1504/IJEP.2011.038443>
- Frederix, E. M. A., Kuczaj, A. K., Nordlund, M., Veldman, A. E. P., & Geurts, B. J. (2017). Eulerian modeling of inertial and diffusional aerosol deposition in bent pipes. *Computers & Fluids*, 159, 217–231. <https://doi.org/10.1016/j.compfluid.2017.09.018>
- Frederix, E. (2016). *Eulerian modeling of aerosol dynamics* [University of Twente]. <https://doi.org/10.3990/1.9789036542289>
- Girimaji, S., & Abdol-Hamid, K. (2005). Partially-Averaged Navier Stokes Model for Turbulence: Implementation and Validation. *43rd AIAA Aerospace Sciences Meeting and Exhibit, January 2005*, 1–14. <https://doi.org/10.2514/6.2005-502>
- Gousseau, P., Blocken, B., & van Heijst, G. J. F. (2011). CFD ymulation of pollutant dispersion around isolated buildings: On the role of convective and turbulent mass fluxes in the prediction accuracy. *Journal of Hazardous Materials*, 194, 422–434. <https://doi.org/10.1016/j.jhazmat.2011.08.008>
- Haghighifard, H. R., Tavakol, M. M., & Ahmadi, G. (2018). Numerical study of fluid flow and particle dispersion and deposition around two inline buildings. *Journal of Wind Engineering and Industrial Aerodynamics*, 179(June), 385–406. <https://doi.org/10.1016/j.jweia.2018.06.018>
- Hao, Z., & Gorlé, C. (2022). Conceptual model to quantify uncertainty in steady-RANS dissipation closure for turbulence behind bluff bodies. *Physical Review Fluids*, 7(1), 14607. <https://doi.org/10.1103/PhysRevFluids.7.014607>
- Irwin, H. P. A. (1979). Design and use of spires for natural wind simulation. *National Aeronautical Establishment, Laboratory Technical Report*.
- Karttunen, S., Kurppa, M., Auvinen, M., Hellsten, A., & Järvi, L. (2020). Large-eddy simulation of the optimal street-tree layout for pedestrian-level aerosol particle concentrations – A case study from a city-boulevard. *Atmospheric Environment: X*, 6(March). <https://doi.org/10.1016/j.aeoa.2020.100073>
- Kato, M., & Launder, B. E. (1993). The modelling of turbulent flow around stationary and vibrating cylinders. *Ninth Symposium on Turbulent Shear Flows*, May.
- Lee, I.-B., Kang, C., Lee, S., Kim, G., Heo, J., & Sase, S. (2004). Development of vertical wind and turbulence profiles of wind tunnel boundary layers. *Transactions of the ASAE*, 47(5), 1717–1726. <https://doi.org/10.13031/2013.17614>
- Leitl, B., & Schatzmann, M. (2005). *CEdVAL at Hamburg University Compilation of Experimental Data for Validation of Microscale Dispersion Models*. <https://mi-pub.cen.uni-hamburg.de/index.php?id=429>
- Liu, S., & Deng, Z. (2023). Transmission and infection risk of COVID-19 when people coughing in an elevator. *Building and Environment*, 238, 110343. <https://doi.org/10.1016/j.buildenv.2023.110343>
- Liu, J., & Niu, J. (2019). Delayed detached eddy simulation of pedestrian-level wind around a building array – The potential to save computing resources. *Building and Environment*, 152(January), 28–38. <https://doi.org/10.1016/j.buildenv.2019.02.011>
- Liu, S., Pan, W., Zhao, X., Zhang, H., Cheng, X., Long, Z., & Chen, Q. (2018). Influence of surrounding buildings on wind flow around a building predicted by CFD simulations. *Building and Environment*, 140(February), 1–10. <https://doi.org/10.1016/j.buildenv.2018.05.011>
- Liu, S., Koupriyanov, M., Paskaruk, D., Fediuk, G., & Chen, Q. (2022). Investigation of airborne particle exposure in an office with mixing and displacement ventilation. *Sustainable Cities and Society*, 79, 103718. <https://doi.org/10.1016/j.scs.2022.103718>
- Liu, Z., Yu, Z., Chen, X., Cao, R., & Zhu, F. (2020). An investigation on external air-flow around low-rise building with various roof types: PIV measurements and LES simulations. *Building and Environment*, 169(November 2019), 106583. <https://doi.org/10.1016/j.buildenv.2019.106583>
- OpenCFD Ltd. (2020). *OpenCFD Release OpenFOAM® v2012*. <https://www.openfoam.com/news/main-news/openfoam-v20-12>
- Manninen, M., Taivassalo, V., & Kallio, S. (1996). *On the mixture model for multiphase flow* (p. 288). VTT Publications.
- Mirzaei, P. A. (2021). CFD modeling of micro and urban climates: Problems to be solved in the new decade. *Sustainable Cities and Society*, 69(November 2020), 102839. <https://doi.org/10.1016/j.scs.2021.102839>
- Mochida, A., Tominaga, Y., Murakami, S., Yoshie, R., Ishihara, T., & Ooka, R. (2002). Comparison of various k-ε models and DSM applied to flow around a high-rise building – Report on AIJ cooperative project for CFD prediction of wind environment. *Wind and Structures, An International Journal*, 5(2–4), 227–244. https://doi.org/10.12989/was.2002.5.2_3_4.227
- Nicoud, F., & Ducros, F. (1999). Subgrid-scale stress modelling based on the square of the velocity gradient tensor. *Flow, Turbulence and Combustion*, 62(3), 183–200. <https://doi.org/10.1023/A:1009995426001>
- Niu, H., Wang, B., Liu, B., Liu, Y., Liu, J., & Wang, Z. (2018). Numerical simulations of the effect of building configurations and wind direction on fine particulate matters dispersion in a street canyon. *Environmental Fluid Mechanics*, 18(4), 829–847. <https://doi.org/10.1007/s10652-017-9563-7>
- Oettl, D. (2015). Evaluation of the Revised Lagrangian Particle Model GRAL Against Wind-Tunnel and Field Observations in the Presence of Obstacles. *Boundary-Layer Meteorology*, 155(2), 271–287. <https://doi.org/10.1007/s10546-014-9993-4>
- Okaze, T., Kikumoto, H., Ono, H., Imano, M., Ikegaya, N., Hasama, T., Nakao, K., Kishida, T., Tabata, Y., Nakajima, K., Yoshie, R., & Tominaga, Y. (2021). Large-eddy simulation of flow around an isolated building: A step-by-step analysis of influencing factors on turbulent statistics. *Building and Environment*, 202(June), 108021. <https://doi.org/10.1016/j.buildenv.2021.108021>
- Putnam, A. (1961). Integratable form of droplet drag coefficient. In *Journal of the American Rocket Society* (Vol. 31, Issue 10, pp. 1467–1468).
- Richards, P. J., & Hoxey, R. P. (1993). Appropriate boundary conditions for computational wind engineering models using the k-ε turbulence model. *Computational Wind Engineering*, 47(C), 145–153. <https://doi.org/10.1016/B978-0-444-81688-7.50018-8>
- Stathopoulos, T., Lazure, L., Saathoff, P., & Gupta, A. (2004). *The effect of stack height, stack location and rooftop structures on air intake contamination: a laboratory and full-scale study*. IRSST.
- Toja-Silva, F., Peralta, C., Lopez-Garcia, O., Navarro, J., & Cruz, I. (2015). Roof region dependent wind potential assessment with different RANS turbulence models. *Journal of Wind Engineering and Industrial Aerodynamics*, 142, 258–271. <https://doi.org/10.1016/j.jweia.2015.04.012>
- Tominaga, Y. (2015). Flow around a high-rise building using steady and unsteady RANS CFD: Effect of large-scale fluctuations on the velocity statistics. *Journal of Wind Engineering and Industrial Aerodynamics*, 142, 93–103. <https://doi.org/10.1016/j.jweia.2015.03.013>
- Tominaga, Y., & Stathopoulos, T. (2007). Turbulent Schmidt numbers for CFD analysis with various types of flowfield. *Atmospheric Environment*, 41(37), 8091–8099. <https://doi.org/10.1016/j.atmosenv.2007.06.054>
- Tominaga, Y., & Stathopoulos, T. (2010). Numerical simulation of dispersion around an isolated cubic building: Model evaluation of RANS and LES. *Building and Environment*, 45(10), 2231–2239. <https://doi.org/10.1016/j.buildenv.2010.04.004>
- Tominaga, Y., & Stathopoulos, T. (2017). Steady and unsteady RANS simulations of pollutant dispersion around isolated cubical buildings: Effect of large-scale fluctuations on the concentration field. *Journal of Wind Engineering and Industrial Aerodynamics*, 165(February), 23–33. <https://doi.org/10.1016/j.jweia.2017.02.001>
- Tominaga, Y., Mochida, A., Yoshie, R., Kataoka, H., Nozu, T., Yoshikawa, M., & Shirasawa, T. (2008). AIJ guidelines for practical applications of CFD to pedestrian wind environment around buildings. *Journal of Wind*

- Engineering and Industrial Aerodynamics*, 96(10–11), 1749–1761. <https://doi.org/10.1016/j.jweia.2008.02.058>
- Trini Castelli, S., Armand, P., Tinarelli, G., Duchenne, C., & Nibart, M. (2018). Validation of a Lagrangian particle dispersion model with wind tunnel and field experiments in urban environment. *Atmospheric Environment*, 193(July), 273–289. <https://doi.org/10.1016/j.atmosenv.2018.08.045>
- Vardoulakis, S., Dimitrova, R., Richards, K., Hamlyn, D., Camilleri, G., Weeks, M., Sini, J. F., Britter, R., Borrego, C., Schatzmann, M., & Moussiopoulos, N. (2011). Numerical Model Inter-comparison for Wind Flow and Turbulence Around Single-Block Buildings. *Environmental Modeling and Assessment*, 16(2), 169–181. <https://doi.org/10.1007/s10666-010-9236-0>
- Wu, J., Xiao, H., Sun, R., & Wang, Q. (2019). Reynolds-averaged Navier-Stokes equations with explicit data-driven Reynolds stress closure can be ill-conditioned. *Journal of Fluid Mechanics*, 869, 553–586. <https://doi.org/10.1017/jfm.2019.205>
- Yoshie, R., Mochida, A., Tominaga, Y., Kataoka, H., Harimoto, K., Nozu, T., & Shirasawa, T. (2007). Cooperative project for CFD prediction of pedestrian wind environment in the Architectural Institute of Japan. *Journal of Wind Engineering and Industrial Aerodynamics*, 95(9–11), 1551–1578. <https://doi.org/10.1016/j.jweia.2007.02.023>
- Zhao, B., Chen, C., & Tan, Z. (2009). Modeling of ultrafine particle dispersion in indoor environments with an improved drift flux model. *Journal of Aerosol Science*, 40(1), 29–43. <https://doi.org/10.1016/j.jaerosci.2008.09.001>
- Zhao, R., Liu, S., Liu, J., Jiang, N., & Chen, Q. (2022). Generalizability evaluation of k-ε models calibrated by using ensemble Kalman filtering for urban airflow and airborne contaminant dispersion. *Building and Environment*, 212, 108823. <https://doi.org/10.1016/j.buildenv.2022.108823>
- Zhao, R., Liu, S., Liu, J., Jiang, N., & Chen, Q. (2023). Equation discovery of dynamized coefficients in the k-ε model for urban airflow and airborne contaminant dispersion. *Sustainable Cities and Society*, 99, 104881. <https://doi.org/10.1016/j.scs.2023.104881>
- Zheng, X., & Yang, J. (2021). CFD simulations of wind flow and pollutant dispersion in a street canyon with traffic flow: Comparison between RANS and LES. *Sustainable Cities and Society*, 75(August), 103307. <https://doi.org/10.1016/j.scs.2021.103307>
- Zou, J., Yu, Y., Liu, J., Niu, J., Chauhan, K., & Lei, C. (2021). Field measurement of the urban pedestrian level wind turbulence. *Building and Environment*, 194(February), 107713. <https://doi.org/10.1016/j.buildenv.2021.107713>

Publisher's Note

Springer Nature remains neutral with regard to jurisdictional claims in published maps and institutional affiliations.